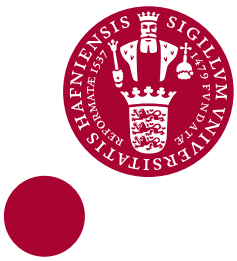

Excited-State Relaxation and Förster Resonance Energy Transfer in an Organic Fluorophore/Silver Nanocluster Dyad

Bogh, Sidsel Ammitzboll; Cerretani, Cecilia; Kacenauskaite, Laura; Carro-Temboury, Miguel R.; Vosch, Tom

Published in:
ACS Omega

DOI:
10.1021/acsomega.7b00582

Publication date:
2017

Document version
Publisher's PDF, also known as Version of record

ACS OMEGA

Article

http://pubs.acs.org/journal/acsodf

Excited-State Relaxation and Förster Resonance Energy Transfer in an Organic Fluorophore/Silver Nanocluster Dyad

Sidsel Ammitzbøll Bogh,[‡] Cecilia Cerretani,[‡] Laura Kacenauskaite, Miguel R. Carro-Temboury, and Tom Vosch*

Nanoscience Center and Department of Chemistry, University of Copenhagen, Universitetsparken 5, 2100 Copenhagen, Denmark

Supporting Information

ABSTRACT: A single-stranded DNA-based (ssDNA) dyad was constructed comprising 15 silver atoms stabilized by a ssDNA scaffold (DNA-AgNC) and an Alexa 546 fluorophore bound to the 5′ end. The Alexa 546 was chosen to function as a Förster resonance energy transfer (FRET) donor for the AgNC. Time-correlated single photon counting (TCSPC) experiments allowed unraveling the excited-state relaxation processes of the purified DNA-AgNC-only system. The TCSPC results revealed slow relaxation dynamics and a red shift of the emission spectrum during the excited-state lifetime. The results from the model systems were needed to understand the more complicated decay pathways present in the collected high-performance liquid chromatography fraction, which contained the dyad (37% of the emissive population). In the dyad system, the FRET efficiency between donor and acceptor was determined to be 94% using TCSPC, yielding a center-to-center distance of 4.6 nm. To date, only limited structural information on DNA-AgNCs is available and the use of TCSPC and FRET can provide information on the center-to-center distance between chromophores and provide positional information in nanostructures composed of AgNCs.

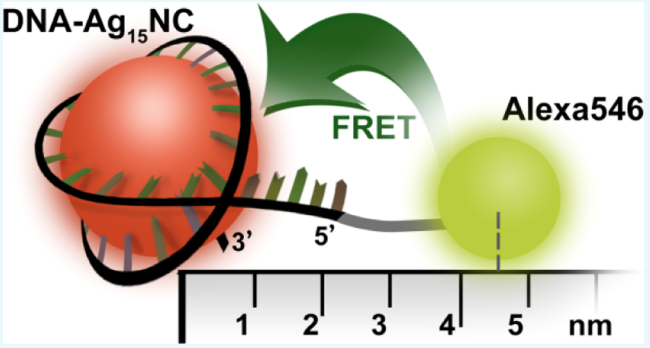

INTRODUCTION

DNA-stabilized fluorescent silver nanoclusters (AgNCs) are a relatively new class of emitters that have found applications in sensing and fluorescence imaging.[1−8] Unlike larger silver nanoparticles that are characterized by plasmon absorption bands, these AgNCs consist of a limited number of atoms (usually below 25 atoms)[9] and display emission throughout the visible and near-infrared (NIR) parts of the electromagnetic spectrum.[10−13] The emission can be tuned by changing the stabilizing scaffold.[14−17] Progress has been made in the preparation and study of DNA-stabilized AgNCs by purifying the as-synthesized samples using high-performance liquid chromatography (HPLC).[11,18−20] This opens up the possibility to use DNA not only as the scaffold that stabilizes the fluorescent AgNC, but also to integrate the emitters at specific positions in nanoscale DNA assemblies.[21,22] HPLC-purified samples, combined with mass spectrometry, allows linking the amount of silver atoms attached to the DNA to the spectral properties, and X-ray based techniques can provide further structural details.[11,20,23−28] Despite the boom in AgNC-fluorescence-based applications, fundamental studies that investigate the individual spectral properties of the purified emitters are limited. Even more limited are studies on the interaction with other classic organic fluorophores (e.g., as a Förster resonance energy transfer (FRET) pair).[21,29] FRET pairs have been used to study protein structure and provide positional information.[30] By constructing a dye−AgNC FRET pair with a controlled position of the dye, positional information on the AgNC could be unraveled, providing valuable information in the field of DNA-AgNCs until full structural elucidation by X-ray techniques is available. In this article, we study the spectroscopic properties of a red-emitting AgNC that was purified by HPLC and investigate the effect of the presence of an organic fluorophore (Alexa 546) linked to the 5′ end of the DNA scaffold (5′-CACCGCTTTTGCCTTTTGGGGACGGATA-3′). The latter creates a DNA-based FRET pair with Alexa 546 as the donor and the AgNC as the acceptor, which we will refer to as the DNA-Alexa546-AgNC dyad (see Scheme 1). An AgNC encapsulated in the same DNA sequence with an additional TTTT linking sequence and a rhodamine attached to the 3′ end was previously studied by Gwinn et al.[21] Their deduced value of R_0 = 7.2 nm together with FRET efficiency ≥67% implies a dye−cluster distance of ≤6.4 nm. Because these values were based on intensity measurements and not from time-correlated single photon counting (TCSPC) measurements, it can only provide a lower limit estimate for the FRET efficiency because the presence of a donor-only fraction cannot be excluded. We demonstrate that the use of TCSPC allows discriminating the dyad from the donor-only fraction and

Received: May 10, 2017
Accepted: August 3, 2017
Published: August 17, 2017

DOI: 10.1021/acsomega.7b00582
ACS Omega 2017, 2, 4657−4664

Scheme 1. Chemical Composition of the Two Model Compounds DNA-Alexa546 (1) and DNA-AgNC (2) and the DNA-Alexa546-AgNC dyad (3)[a]

1) DNA-Alexa546
Alexa546-5′-CACCGCTTTTGCCTTTTGGGGACGGATA-3′

2) DNA-AgNC
5′-CACCGCTTTTGCCTTTTGGGGACGGATA-3′@Ag_{15}

3) DNA-Alexa546-AgNC
Alexa546-5′-CACCGCTTTTGCCTTTTGGGGACGGATA-3′@Ag_{15}

[a]The @ indicates that the AgNC is stabilized by the DNA sequence.

calculating the true FRET efficiency of the dyad. Our study with Alexa 546 at the 5′ end provides additional information that can help to ultimately pin down the position of the AgNC in the DNA strand. The goal here is to determine the FRET efficiency of the pure dyad and hence determine the center-to-center distance between the donor and acceptor using Förster's point dipole approximation.[31] The latter has so far not been done experimentally and will provide important information regarding future nanoscale assemblies using AgNCs and in determining the actual position of the AgNC in the stabilizing DNA scaffold. To fully disentangle the photophysical properties of the dyad, we first investigate the two subsystems individually. These two model systems are DNA-Alexa546 and DNA-AgNC (see Scheme 1). Particularly, the understanding of the TCSPC behavior of the AgNC fluorescence was found to be important. The solvatochromism of DNA-AgNCs has been discussed recently in the literature together with the potential use of the fluorescence sensing in DNA studies.[32−34] It has been shown (and in particular for this sequence of DNA) that nonspecific solvent interaction models are not applicable to DNA-AgNCs. Instead, solvent-induced structural changes and/or dielectric changes in the local vicinity of the clusters have been proposed as plausible explanations.[34] Furthermore, the refractive index sensitivity of these DNA-AgNCs tested in glycerol/water mixtures was suggested to reflect local dielectric variations.[32] Additionally, time-dependent spectral shifts on the nanosecond time scale have been studied via time-resolved emission spectra (TRES) by Hsu et al., suggesting solvation dynamics near the DNA bases.[33] The later was done however on as-synthesized samples without purification. Besides these relaxations on the pico- and nanosecond time scales, the ultrafast relaxation from the absorptive state to the emissive state of NIR-emitting DNA-AgNCs was shown to occur within 140 fs.[35] The characterization of the relaxation dynamics and the interpretation of the TCSPC data will help future studies and the use of DNA-AgNCs in FRET applications.

RESULTS AND DISCUSSION

DNA-Alexa546. We start our investigation by looking at the steady-state and time-resolved photophysical properties of Alexa 546 linked to the DNA sequence that will later be used to stabilize the AgNC in the dyad system (see Scheme 1). The absorption and emission spectra of DNA-Alexa546 can be found in Figure 1A. DNA-Alexa546 has an absorption maximum at 555 nm and an emission maximum at 571 nm in 10 mM ammonium acetate buffer (NH_4OAc). These values are similar to the values provided by the manufacturer of Alexa 546 (556 and 573 nm, respectively).[36] A two-dimensional (2D) excitation versus emission plot of DNA-Alexa546 can be found in Figure S1. The fluorescence quantum yield of DNA-

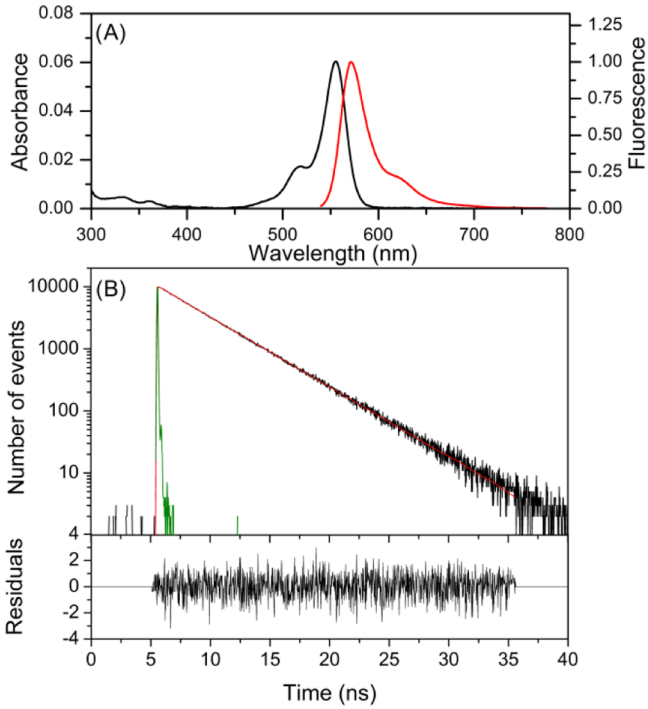

Figure 1. (A) Absorption (black curve, left *Y* axis) and normalized emission spectra of DNA-Alexa546 (red curve, right *Y* axis, excited at 510 nm). (B) Fluorescence decay of DNA-Alexa546 excited at 507 nm, detected at 570 nm (black curve). The decay curve was fitted with a biexponential decay model (red curve). The green curve is the IRF. The biexponential model had a reduced χ^2 of the fit of 0.899.

Alexa546 was measured to be 0.84 using Rhodamine 6G in absolute ethanol (fluorescence quantum yield = 0.95) as a reference.[37−39] This value is also similar to the value of the succinimidyl ester derivative in aqueous solution reported by the manufacturer (0.79).[40] TCSPC experiments show that the fluorescence decay curve of DNA-Alexa546 excited at 507 nm and detected at 570 nm can be best fitted with a biexponential model (see Figure 1B). Fractional intensities of 99% (3.87 ± 0.01 ns decay component) and 1% (1.37 ± 0.48 ns decay component) were found, indicating that the fluorescence can be considered to be mainly coming from one emissive species with a decay time of 3.87 ns, which is similar to the decay time of 4.1 ns reported by the manufacturer.[40] Analyzing decay curves over the whole Alexa 546 emission range allows constructing TRES. The TRES in Figure S2 shows no shift on time scales slower than the instrument response function (IRF). The steady-state and time-resolved experiments on DNA-Alexa546 show that the fluorophore behaves as expected and no unwanted quenching or spectral changes occurred upon conjugation to the DNA. During the cluster formation process in the DNA-Alexa546-AgNC dyad, $NaBH_4$ is used for reduction of the silver cations. We tested whether addition of $NaBH_4$ to DNA-Alexa546 has an effect on the chemical stability of the fluorophore. Figure S3 shows that addition of similar amounts of $NaBH_4$ used for the reduction of the silver cations has a neglectable effect on the UV−vis absorption spectrum of DNA-Alexa546.

DNA-AgNC. In a next step, we studied the photophysical properties of the DNA-AgNC in detail. The sequence was investigated previously and has been reported to stabilize 15 Ag atoms.[21,22,26,27,32,34,41] After synthesis, the DNA-AgNC sample was purified by HPLC. For this, the fraction around 7.7 min

DOI: 10.1021/acsomega.7b00582
ACS Omega 2017, 2, 4657−4664

that shows absorption at 600 nm (see Figure S4) was collected. Figure 2A shows the absorption, excitation, and emission

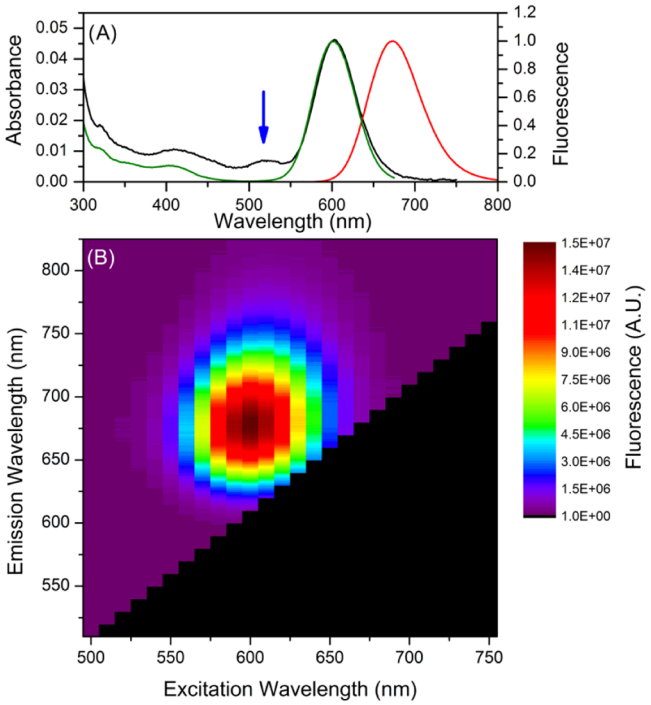

Figure 2. (A) Absorption (black curve, left *Y* axis), excitation (green curve, right *Y* axis, detected at 700 nm), and emission (red curve, right *Y* axis, excited at 561 nm) spectra of the DNA-AgNC. The blue arrow indicates the absorption feature that is not present in the excitation spectrum. (B) Two-dimensional excitation vs emission plot of the DNA-AgNC.

spectra of DNA-AgNC. The absorption maximum is at 603 nm, whereas the emission maximum is at 672 nm. Recording an excitation spectrum monitoring the emission at 700 nm reveals that most of the features of the absorption spectrum can be found in the excitation spectrum as well. The main difference is the peak around 510 nm (indicated by a blue arrow), which is absent in the excitation spectrum, indicating that this absorption feature is not related to the emissive AgNC with a maximum at 672 nm. Additionally, the absorption spectrum has a broader tail in the 650−700 nm region. The latter indicates that besides the main emissive species at 600 nm, even after HPLC purification, a number of additional absorbing species are present, both blue- and red-shifted. Upon closer investigation of the absorption spectra recorded during HPLC purification, it can be seen that these additional species are more pronounced in the tail of the peak of the fraction collected around 7.7 min compared to the maximum (see Figure S5). Figure S5 indicates that it is possible to increase the purity by avoiding the tail fraction. However, Figure 2B shows that the purified DNA-AgNC fraction can still be described as mainly one single emitter and that these other absorbing species do not contribute significantly to the fluorescence. Additionally, photobleaching experiments show that even if one collects a single pure fraction, this fraction can be photo-converted into the other species (see Figure S6). The fluorescence quantum yield of the AgNC with an emission maximum at 672 nm was measured to be 0.68 using cresyl violet in ethanol as a reference.[37,39,42] This is in good agreement with the value of 0.75 reported by the group of Gwinn et al.[21,26] Fluorescence correlation spectroscopy (FCS) was used to estimate the molar extinction coefficient of the DNA-AgNC.[43] A value of 1.5E5 M^{-1} cm^{-1} was found using Atto633 as a reference dye for volume estimation (see Figure S7). Although this value, determined by FCS, should be considered an estimate, it matches well with the estimate provided by Gwinn et al. of 1.4E5 M^{-1} cm^{-1}, which was based on purity estimation and comparison to the estimated DNA molar extinction coefficient.[21,44,45]

After having analyzed the steady-state properties, we performed TCSPC experiments on the DNA-AgNC sample. Despite the fact that steady-state 2D plot indicates a single emitter, the fluorescence decay curves when excited at 561 nm do not fit satisfactory to a monoexponential decay model. At least a triexponential model is needed to get a satisfactory global fit of decay curves at different emission wavelengths. Figure S8 shows the decay-associated spectra (DAS) of the three decay components. A dominant component of 3.95 ns is present that has DAS similar to the steady-state spectrum. The two additional decay components have DAS with blue-shifted maxima and positive amplitudes at short wavelengths and negative amplitudes at long wavelengths. The DAS in Figure S8 represent the typical signature of a time-dependent relaxation during the excited-state decay.[46−48] As a result of the relatively slow relaxation, the emission red-shifts during the time that it takes for the AgNCs to decay back to the ground state. To illustrate this point better, the same data can be plotted in TRES form. Figure 3A shows the TRES at different points in

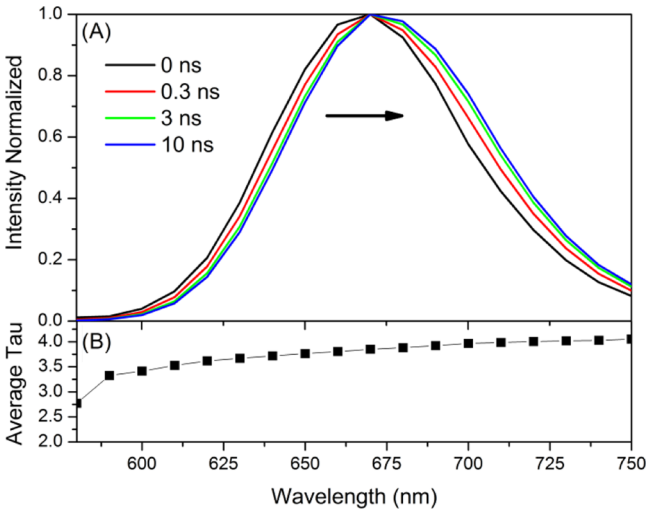

Figure 3. (A) Time-resolved emission spectra of the DNA-AgNC. The black arrow indicates that the emission spectrum shifts bathochromically with time. (B) Average decay time of the DNA-AgNC as a function of emission wavelength.

time after excitation. A clear red shift can be observed as indicated by the black arrow. This phenomenon can also be clearly seen in the average decay time spectrum[49] and results in an increase in the average decay time with increasing emission wavelength (see Figure 3B). So, despite the apparent complicated multiexponential decay behavior, the system can be satisfactorily described as one emissive species that displays excited-state relaxation and hence red-shifts on the time scale of the fluorescence decay time. A similar behavior was also reported by Hsu et al. for a green-emissive AgNC.[33] To investigate this relaxation in more detail, we fitted the TRES

DOI: 10.1021/acsomega.7b00582
ACS Omega 2017, 2, 4657−4664

data points with a Gaussian function and plotted the evolution of the emission maximum as a function of time. The latter can be seen in Figures S9 and S10. The shift in the position of the emission maximum can be satisfactory fitted by a biexponential decay model with time constants of 0.2 and 4.1 ns. The similarity to the results reported by Hsu et al. could indicate that this is a universal feature of the DNA-stabilized AgNC, potentially linked to relaxation dynamics of the DNA scaffold.[50,51] It is also interesting to point out that Andreatta et al. showed that for a Coumarin chromophore that was embedded in the DNA structure, the solvation dynamics stretched well into the nanosecond range, whereas for the same chromophore, this was done in 10 ps in pure water.[50] We found a time-dependent Stokes shift of ca. 160 cm^{-1}, which is shorter than the value of ca. 700 cm^{-1} in water found by Hsu et al. The latter could be due to the different DNA sequence used and to the higher purity of our sample. Experiments on purified samples would minimize the contribution of multiple species to the energy shift. Further detailed TCSPC experiments changing temperature or viscosity of the solvent could provide valuable insight.

DNA-Alexa546-AgNC Dyad. Now that the Alexa 546 donor and AgNC acceptor have been photophysically characterized, we synthesized the DNA-Alexa546-AgNC dyad. Details of the synthesis can be found in the Materials and Methods section. After HPLC purification, the DNA-Alexa546-AgNC dyad was retrieved, but the sample still contained other components (see Figure S11, the broad 555 nm absorption with a peak maximum at 13 min is also present at 10 min, where the dyad fraction that absorbs at 625 nm is collected). Figure S12 shows the absorption spectra at 10 and 13 min elution times, where the spectral feature of the dyad can be seen at 10 min. The fraction eluting at 13 min contained the spectral features of DNA and Alexa546 and most likely has a number of silver atoms bound to the DNA (however nonemissive and without significant absorption features in the visible range) because the elution time is different from that of the DNA-Alexa546 starting compound without silver (see Figure S13). Figure 4A shows the absorption, emission, and excitation spectra of the collected DNA-Alexa546-AgNC dyad fraction. The absorption spectrum (black curve) shows the presence of the two absorption features of Alexa 546 and the AgNC with maxima at 555 and 603 nm, respectively. The excitation spectrum (green curve), monitoring predominantly the AgNC emission at 710 nm, also indicates that there is energy transfer from Alexa 546 to the AgNC. The emission spectrum (red curve), exciting predominantly Alexa 546 at 510 nm, also indicates energy transfer because significant emission from the AgNC is present. The presence of the energy transfer can also be seen in the 2D plot in Figure 4B, where excitation of the donor at 560 nm leads to significant emission of the AgNCs at 670 nm. The choice of Alexa 546 gives a less congested 2D excitation versus emission map due to the lower overlap between donor emission and acceptor emission compared to the rhodamine used in a previous study.[21] Similar to what we observed for the pure DNA-AgNC, exposure to light leads to a reduction of the AgNC emission at 670 nm in the dyad system (see Figure S14). A 2D plot like Figure 4B can show the presence of FRET but cannot be used to determine the efficiency because one cannot exclude the presence of a donor-only fraction and an acceptor-only fraction (the latter is unlikely as Figure S13 indicates that there is no significant amount of DNA without Alexa 546).[21]

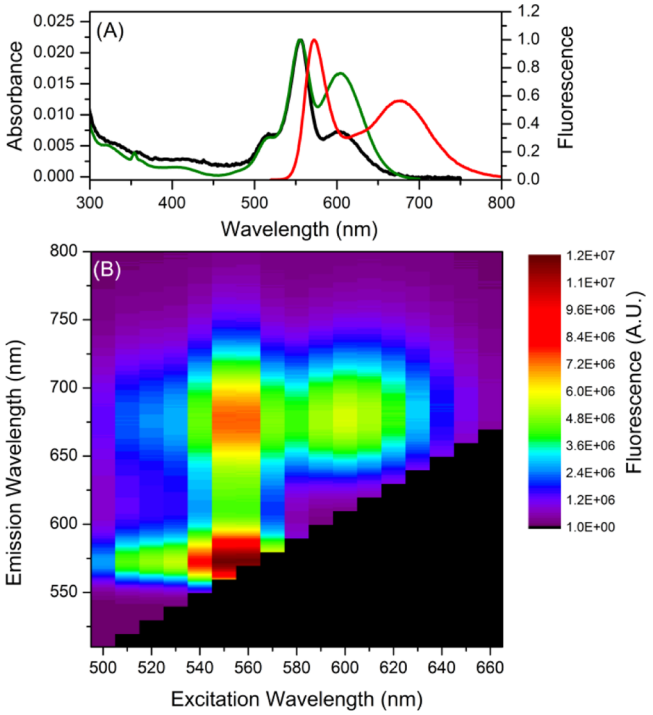

Figure 4. (A) Absorption (black curve, left *Y* axis), excitation (green curve, right *Y* axis, detected at 710 nm), and emission (red curve, right *Y* axis, excited at 510 nm) spectra of the dyad. (B) Two-dimensional excitation vs emission plot of the DNA-Alexa546-AgNC dyad.

We therefore performed TCSPC experiments, exciting the Alexa 546 at 507 nm (at this wavelength, there is very little direct excitation of the acceptor; see green curve in Figure 2A and Supporting Information). The TCSPC data for the DNA-Alexa546-AgNC dyad fraction could be best fitted with a triexponential model. The DAS of the three components can be found in Figure 5A. Of the three decay components, two were globally linked, whereas one decay component, tau 1, was kept variable. The evolution of tau 1 as a function of emission

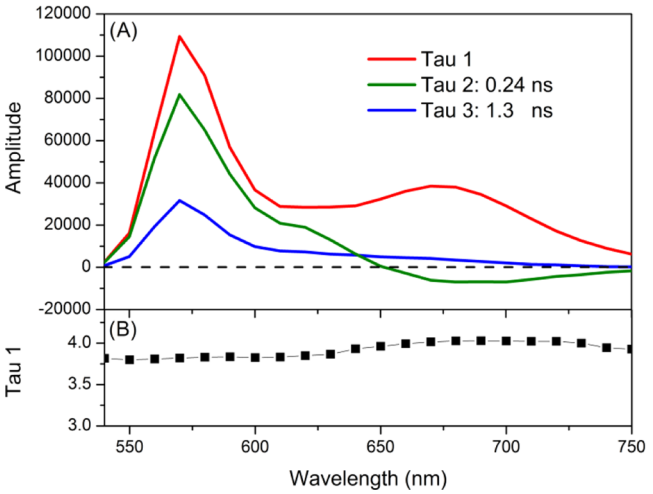

Figure 5. (A) DAS of the collected DNA-Alexa546-AgNC dyad sample. The represented amplitudes are preexponential factors used in the triexponential fit. Tau 2 and 3 were globally linked in the fit. The dashed black line is a guide showing the zero line. (B) Decay time value of tau 1 as a function of emission wavelength. Tau 1 was not globally linked in the fit.

DOI: 10.1021/acsomega.7b00582
ACS Omega 2017, 2, 4657−4664

wavelength can be seen in Figure 5B. As discussed in the previous sections, the decay time of Alexa 546 is 3.87 ns and that of the DNA-AgNC is wavelength dependent, roughly between 3.2 and 4 ns. Because the fluorescence lifetimes of the donor and the acceptor are so similar and thus very hard to separate in a data fit, we took the approach not to link tau1 globally so that this decay term could represent both the decay of the Alexa 546 in the absence of a FRET acceptor and the AgNC emission. Linking tau 1 globally gives unsatisfactory fits, so does a four exponential globally linked fit. The latter is due to the changing decay time of the AgNC emission as a function of wavelength and the similarity in the decay times of Alexa 546 and AgNC. However, the model that we used here represents the fluorescence decay behavior of the dyad system well. In the wavelength range of 540−610 nm, tau 1 is fairly constant around 3.82 ns, representing predominantly the Alexa 546 donor-only decay. This must come from a fraction of DNA-Alexa546 that has silver atoms bound to it but did not form a cluster that is able to quench the emission of the Alexa 546 fluorophore. Figure S13 indicates that it is unlikely that we collect the DNA-Alexa546 starting compound at these elution times. From 610 to 720 nm, the decay time steadily increases as was also observed for the DNA-AgNC in Figure 3B. For the last three points from 730 to 750 nm, the decay time drops again slightly. The reason for this is not clear at the moment. Looking at the DAS, we can confidently attribute tau 1 to the combination of the decay of two compounds: one is from an Alexa 546 without an AgNC acceptor and the other is AgNC emission from a DNA-Alexa546-AgNC dyad excited through FRET. The FRET from Alexa 546 to the AgNC is evidenced by the 0.24 ns decay component, which for the positive amplitude part has the spectral shape of the Alexa 546 and for the negative amplitude part has the spectral shape of the DNA-AgNC. The fact that Alexa 546 decays with a time constant of 0.24 ns and the emission of the AgNC rises/appears with the same time constant proves without any doubt the presence of the FRET process (see Figure 5A).[52] On the basis of the energy-transfer decay time and the decay time of DNA-Alexa546, a FRET efficiency of 94% for the DNA-Alexa546-AgNC dyad can be calculated. Due to the fact that the energy-transfer time is approaching the IRF's full width at half-maximum (FWHM), one could also consider it as a lower limit; however, we used numerical reconvolution analysis of the decay curves, which can resolve features well below the IRF's FWHM.[53] The molar extinction coefficient determined from the FCS can be used to calculate the spectral overlap between the Alexa 546 donor and the AgNC acceptor. An R_0 value of 7.34 nm is found using a κ^2 value of 2/3. The value of 2/3 is a good estimate looking at the anisotropy in the DNA-Alexa546-AgNC dyad in a 95% glycerol solution at room temperature, where the mobility of the dyad should be severely limited by the high viscosity of the solvent. Figure S15A shows that a value of 0.06 was found in the donor excitation region, which is close to 0 and hence the relative orientation of the donor and acceptor dipoles can be considered close to random. We note that the random relative orientation of the dipoles is due to the ensemble averaging of the different orientations and not due to fast segmental rotation of the donor and acceptor because the anisotropy is measured in glycerol. Indeed, a value of 0.37 is found in the acceptor region (close to the maximum value of 0.4 indicating virtually no depolarization). In water, segmental rotation of the donor and acceptor would be enabled, justifying even more the use of $\kappa^2 = 2/3$.[46] We note that the long linking chain between the Alexa 546 chromophore and the DNA strand should provide conformational flexibility (see Scheme S1). The emission anisotropy, exciting the AgNC in the DNA-Alexa546-AgNC dyad, is around 0.38 and constant over the emission range (see Figure S15B). On the basis of the efficiency of energy transfer and the R_0 value, we can estimate the center-to-center distance of the FRET pair.[46] This leads to a value of 4.6 nm. Overall, we can conclude that very efficient energy transfer from Alexa 546 to the AgNC is present in the DNA-Alexa546-AgNC dyad and that they are 4.6 nm separated from each other. Follow-up FRET experiments increasing the distance and hence lowering the energy-transfer rate would be interesting to test the accuracy of our distance determination. The third decay component in Figure 5A has a decay time of 1.3 ns, and the DAS has the spectral shape of Alexa 546. This decay time seems to be related to an Alexa 546 chromophore that has a reduced decay time but does not transfer energy to another emissive state because no negative amplitude is observed at long wavelengths. The origin of the reduced decay time is not clear. Two possible explanations can be proposed. One is the quenching of Alexa 546 by silver ions or nonemissive silver nanoclusters in the DNA scaffold. Another explanation could be quenching by a specific DNA base. We noticed that DNA-Alexa546 has a minor fractional intensity contribution of 1% of a 1.37 ± 0.48 ns decay component. One could speculate that the binding of silver to DNA could change the conformation of the DNA and force the Alexa 546 in a position where it is on average more often in proximity to a quenching DNA base. Previous results have shown that Alexa 546 is most efficiently quenched by guanine.[54] Exciting at 507 nm and looking at the decay amplitudes at 570 nm, we can determine three decay pathways in the collected DNA-Alexa546-AgNC dyad fraction. A proportion of 49% of the excited Alexa 546 chromophores decay with the normal decay time around 3.82 ns, indicating that no AgNC acceptor is present, and 37% of the Alexa 546 chromophores undergo efficient FRET (94% efficiency) to the AgNC acceptor. The remaining 14% Alexa 546 chromophores decay with a reduced decay time of 1.3 ns. Despite the presence of a mixture of compounds in the collected fraction, TCSPC can untangle the components and determine the efficiency of the DNA-Alexa546-AgNC dyad fraction.

At the moment, we cannot resolve the degree of folding of the DNA, but this study opens the possibility of deducing it by pinning down the center-to-center value with further FRET studies. The most accurate distance determination would be for a FRET pair with a distance difference of R_0, where the change in energy-transfer efficiency is most sensitive to the donor acceptor distance.[46] For the same DNA-AgNC, this can be achieved using a different donor dye with a worse spectral overlap. Another different/complementary approach would be adding a longer rigid linker with a short flexible end between the same DNA sequence and donor dye.

CONCLUSIONS

In this study, a detailed analysis of the decay pathways of the collected DNA-Alexa546-AgNC dyad fraction after HPLC purification is presented. For the Alexa546-AgNC dyad, efficient FRET (94% efficiency) is present and a center-to-center distance between the two chromophores of 4.6 nm was calculated. This study demonstrates the possibility of determining the average center-to-center distance between the AgNC and another fluorophore attached to the DNA. In the future, systematic variations of the distance between donor

DOI: 10.1021/acsomega.7b00582
ACS Omega 2017, 2, 4657−4664

and acceptor (by varying the number of bases in the stabilizing single-stranded DNA (ssDNA)), or changing the donor dye (and thereby the spectral overlap), could lead to an accurate position determination of the AgNC chromophore inside the DNA.[30] Additionally, we show that the AgNC emission displays a shift in the emission spectrum on the time scale of the excited-state decay time. This leads to multiexponential decay behavior at fixed emission wavelengths and complicated DAS. However, a simpler picture emerges when the same data are analyzed using TRES. In this way, the emission spectrum can be seen shifting and the emission maxima can be fitted with a biexponential shift model with shift times of 0.2 and 4.1 ns. Further follow-up experiments changing temperature or viscosity of the solvent could provide insight into the origin of these relaxation dynamics, which could be related to the DNA scaffold.[33,34,50]

MATERIALS AND METHODS

Sample Preparation. DNA-AgNC and the DNA-Alexa546-AgNC dyad were synthesized by mixing hydrated DNA or DNA-Alexa546 (both from IDT technologies) with $AgNO_3$ (99.9999%, Sigma-Aldrich) in a solution of 10 mM ammonium acetate (NH_4OAc) in nuclease-free water from IDT technologies. After 15 min, the silver ions were reduced with 0.5 equiv of $NaBH_4$ (99.99%, Sigma-Aldrich). The concentration ratio of ssDNA/$AgNO_3$/$NaBH_4$ (in μM) in the final mixture was 15:187.5:93.75. The samples were left at room temperature overnight and were concentrated ∼8× using spin filtration (Amicon Ultra-2 Centrifugal Filter Unit with Ultracel-3 membrane) before injection in the HPLC system. After HPLC purification, all samples were solvent-exchanged by spin filtration into 10 mM NH_4OAc before any measurements. HPLC-purified ssDNA with an Alexa Fluor 546 linked at the 5′ end (NHS ester linking) was purchased from IDT technologies (see Scheme S1 for details on the linker structure).

HPLC Purification. HPLC purification was done using a preparative HPLC system from Agilent Technologies with an Agilent Technologies 1260 infinity fluorescence detector and a Kinetex C18 column (5 μm, 100 Å, 50 × 4.6 mm^2) and a linear gradient flow of 35 mM triethylammonium acetate (TEAA) in water/MeOH. For DNA-AgNC (eluting at ∼21% TEAA in MeOH), the gradient was varied from 15 to 30% TEAA in methanol in 15 min and fractions were collected using the absorbance signal at 600 nm. For the DNA-Alexa546-AgNC dyad (eluting at ∼39% TEAA in MeOH), the gradient was varied from 35 to 50% TEAA in methanol in 30 min and fractions were collected using the absorbance signal at 625 nm to diminish signal from Alexa 546. The flow rate was 1.5 mL/min in both cases. All HPLC gradients were followed by 6 min of washing with 95% TEAA in methanol to remove any remaining sample from the column.

Steady-State Absorption and Emission Spectroscopy. All absorption measurements were carried out on a Lambda1050 instrument from PerkinElmer using a deuterium lamp for ultraviolet radiation and a halogen lamp for visible and near-infrared radiation. Steady-state fluorescence measurements were done either using a FluoTime300 instrument from PicoQuant with a 507 nm laser or a 561 nm laser as excitation source or using a QuantaMaster400 from PTI with a xenon arc lamp as excitation source. All fluorescence spectra were corrected for the wavelength dependency of the detector system.

Anisotropy Measurements. Steady-state anisotropy measurements were carried out in a solution of 95% glycerol and 5% 10 mM NH_4OAc at room temperature. The polarization of the excitation light and collected fluorescence was controlled with a set of manual polarizers in the PTI QuantaMaster400 system.

Time-Correlated Single Photon Counting. Time-resolved fluorescence measurements were conducted using the FluoTime300 instrument from PicoQuant with a 510 nm laser (actual wavelength, 507 nm) or a 561 nm laser as excitation source. All time-resolved data were analyzed using FluoFit version 4.6 from PicoQuant.

Fluorescence Correlation Spectroscopy. Fluorescence correlation spectroscopy was performed by focusing in a droplet on a cleaned coverslip on top of a confocal microscope. The excitation source was 600 nm pulsed light (77 MHz) selected from a continuum laser (SuperK Extreme EXB-6 with a SuperK SELECT wavelength selector from NKT Photonics, 290 nW measured on the objective). A 600 nm band-pass filter (Semrock FF01-600/14-25) was used to clean up excitation light. The laser beam (a round-top-hat-like beam profile was used) was focused through an Olympus IX71 microscope by the oil immersion objective (Olympus UPLFLN 100×, 1.3 NA). Scattering from the excitation source was removed using a dichroic mirror (Semrock LPD01-633RS) and a long-pass filter (Semrock LP02-633RU-25). The fluorescence signal was collected through a 100 μm pinhole by an avalanche photodiode (APD, PerkinElmer CD3226). The signals from the APD were recorded by an SPC-830 card (Becker & Hickl). Purified DNA-AgNC solutions were diluted in deionized water to cover a wide range of concentrations. Atto633 (BioReagent, Sigma-Aldrich) was diluted in deionized water (concentrations ranging between ∼5.7 and ∼0.63 nM) and used as a reference dye for excitation-volume determination. All of the FCS measurements were performed at room temperature.

ASSOCIATED CONTENT

Supporting Information

The Supporting Information is available free of charge on the ACS Publications website at DOI: 10.1021/acsomega.7b00582.

Chemical structure, 2D excitation versus emission plot, TRES, and additional absorption spectra of DNA-Alexa546; HPLC images, absorption spectra, and bleaching data of DNA-AgNC and DNA-Alexa546-AgNC; FCS data, DAS, and TRES of DNA-AgNC; steady-state anisotropy data of DNA-Alexa546-AgNC (PDF)

AUTHOR INFORMATION

Corresponding Author

*E-mail: tom@chem.ku.dk. Tel: +4535320313.

ORCID

Sidsel Ammitzbøll Bogh: 0000-0001-9827-6205
Miguel R. Carro-Temboury: 0000-0003-2817-9172
Tom Vosch: 0000-0001-5435-2181

Author Contributions

‡S.A.B. and C.C. contributed equally.

Author Contributions

The manuscript was written through contributions of all authors. All authors have given approval to the final version of the manuscript.

DOI: 10.1021/acsomega.7b00582
ACS Omega 2017, 2, 4657−4664

Notes

The authors declare no competing financial interest.

■ ACKNOWLEDGMENTS

T.V., S.A.B., and M.R.C.-T. gratefully acknowledge financial support from the "Center for Synthetic Biology" at Copenhagen University funded by the UNIK research initiative of the Danish Ministry of Science, Technology and Innovation (Grant 09-065274), bioSYNergy, University of Copenhagen's Excellence Programme for Interdisciplinary Research, the Villum Foundation (Project number VKR023115), the Danish Council of Independent Research (Project number DFF-1323-00352), and the Carlsberg Foundation (CF14-0388). C.C. thanks the Erasmus Plus programme and the University of Florence for giving the opportunity to work at T.V.'s research group.

■ REFERENCES

(1) Petty, J. T.; Zheng, J.; Hud, N. V.; Dickson, R. M. DNA-templated Ag nanocluster formation. *J. Am. Chem. Soc.* **2004**, *126*, 5207−5212.
(2) Zhang, L.; Wang, E. Metal nanoclusters: New fluorescent probes for sensors and bioimaging. *Nano Today* **2014**, *9*, 132−157.
(3) Yang, S. W.; Vosch, T. Rapid Detection of MicroRNA by a Silver Nanocluster DNA Probe. *Anal. Chem.* **2011**, *83*, 6935−6939.
(4) Richards, C. I.; Hsiang, J. C.; Senapati, D.; Patel, S.; Yu, J.; Vosch, T.; Dickson, R. M. Optically Modulated Fluorophores for Selective Fluorescence Signal Recovery. *J. Am. Chem. Soc.* **2009**, *131*, 4619−4621.
(5) Antoku, Y.; Hotta, J.-i.; Mizuno, H.; Dickson, R. M.; Hofkens, J.; Vosch, T. Transfection of living HeLa cells with fluorescent polycytosine encapsulated Ag nanoclusters. *Photochem. Photobiol. Sci.* **2010**, *9*, 716−721.
(6) Yu, J.; Choi, S.; Richards, C. I.; Antoku, Y.; Dickson, R. M. Live Cell Surface Labeling with Fluorescent Ag Nanocluster Conjugates. *Photochem. Photobiol.* **2008**, *84*, 1435−1439.
(7) Deng, L.; Zhou, Z.; Li, J.; Li, T.; Dong, S. Fluorescent silver nanoclusters in hybridized DNA duplexes for the turn-on detection of Hg2+ ions. *Chem. Commun.* **2011**, *47*, 11065−11067.
(8) Enkin, N.; Sharon, E.; Golub, E.; Willner, I. Ag nanocluster/DNA hybrids: Functional modules for the detection of nitroaromatic and RDX explosives. *Nano Lett.* **2014**, *14*, 4918−4922.
(9) Gwinn, E.; Schultz, D.; Copp, S. M.; Swasey, S. DNA-Protected Silver Clusters for Nanophotonics. *Nanomaterials* **2015**, *5*, 180−207.
(10) Richards, C. I.; Choi, S.; Hsiang, J. C.; Antoku, Y.; Vosch, T.; Bongiorno, A.; Tzeng, Y. L.; Dickson, R. M. Oligonucleotide-stabilized Ag nanocluster fluorophores. *J. Am. Chem. Soc.* **2008**, *130*, 5038−5039.
(11) Schultz, D.; Gwinn, E. G. Silver atom and strand numbers in fluorescent and dark Ag:DNAs. *Chem. Commun.* **2012**, *48*, 5748−5750.
(12) Petty, J. T.; Nicholson, D. A.; Sergev, O. O.; Graham, S. K. Near-Infrared Silver Cluster Optically Signaling Oligonucleotide Hybridization and Assembling Two DNA Hosts. *Anal. Chem.* **2014**, *86*, 9220−9228.
(13) Sharma, J.; Yeh, H. C.; Yoo, H.; Werner, J. H.; Martinez, J. S. A complementary palette of fluorescent silver nanoclusters. *Chem. Commun.* **2010**, *46*, 3280−3282.
(14) Choi, S.; Dickson, R. M.; Yu, J. Developing luminescent silver nanodots for biological applications. *Chem. Soc. Rev.* **2012**, *41*, 1867−1891.
(15) Latorre, A.; Somoza, A. DNA-Mediated Silver Nanoclusters: Synthesis, Properties and Applications. *ChemBioChem* **2012**, *13*, 951−958.
(16) Sengupta, B.; Ritchie, C. M.; Buckman, J. G.; Johnsen, K. R.; Goodwin, P. M.; Petty, J. T. Base-Directed Formation of Fluorescent Silver Clusters. *J. Phys. Chem. C* **2008**, *112*, 18776−18782.
(17) Gwinn, E. G.; O'Neill, P.; Guerrero, A. J.; Bouwmeester, D.; Fygenson, D. K. Sequence-dependent fluorescence of DNA-hosted silver nanoclusters. *Adv. Mater.* **2008**, *20*, 279−283.
(18) Petty, J. T.; Sergev, O. O.; Kantor, A. G.; Rankine, I. J.; Ganguly, M.; David, F. D.; Wheeler, S. K.; Wheeler, J. F. Ten-Atom Silver Cluster Signaling and Tempering DNA Hybridization. *Anal. Chem.* **2015**, *87*, 5302−5309.
(19) Petty, J. T.; Sergev, O. O.; Nicholson, D. A.; Goodwin, P. M.; Giri, B.; McMullan, D. R. A Silver Cluster-DNA Equilibrium. *Anal. Chem.* **2013**, *85*, 9868−9876.
(20) Petty, J. T.; Fan, C.; Story, S. P.; Sengupta, B.; Sartin, M.; Hsiang, J.-C.; Perry, J. W.; Dickson, R. M. Optically Enhanced, Near-IR, Silver Cluster Emission Altered by Single Base Changes in the DNA Template. *J. Phys. Chem. B* **2011**, *115*, 7996−8003.
(21) Schultz, D.; Copp, S. M.; Markešević, N.; Gardner, K.; Oemrawsingh, S. S. R.; Bouwmeester, D.; Gwinn, E. Dual-Color Nanoscale Assemblies of Structurally Stable, Few-Atom Silver Clusters, As Reported by Fluorescence Resonance Energy Transfer. *ACS Nano* **2013**, *7*, 9798−9807.
(22) Copp, S. M.; Schultz, D. E.; Swasey, S.; Gwinn, E. G. Atomically Precise Arrays of Fluorescent Silver Clusters: A Modular Approach for Metal Cluster Photonics on DNA Nanostructures. *ACS Nano* **2015**, *9*, 2303−2310.
(23) Neidig, M. L.; Sharma, J.; Yeh, H.-C.; Martinez, J. S.; Conradson, S. D.; Shreve, A. P. Ag K-Edge EXAFS Analysis of DNA-Templated Fluorescent Silver Nanoclusters: Insight into the Structural Origins of Emission Tuning by DNA Sequence Variations. *J. Am. Chem. Soc.* **2011**, *133*, 11837−11839.
(24) Petty, J. T.; Sergev, O. O.; Ganguly, M.; Rankine, I. J.; Chevrier, D. M.; Zhang, P. A Segregated, Partially Oxidized, and Compact Ag10 Cluster within an Encapsulating DNA Host. *J. Am. Chem. Soc.* **2016**, *138*, 3469−3477.
(25) Volkov, I. L.; Smirnova, A.; Makarova, A. A.; Reveguk, Z. V.; Ramazanov, R. R.; Usachov, D. Y.; Adamchuk, V. K.; Kononov, A. I. DNA with Ionic, Atomic, and Clustered Silver: An XPS Study. *J. Phys. Chem. B* **2017**, *121*, 2400−2406.
(26) Schultz, D.; Gardner, K.; Oemrawsingh, S. S. R.; Markešević, N.; Olsson, K.; Debord, M.; Bouwmeester, D.; Gwinn, E. Evidence for Rod-Shaped DNA-Stabilized Silver Nanocluster Emitters. *Adv. Mater.* **2013**, *25*, 2797−2803.
(27) Swasey, S. M.; Karimova, N.; Aikens, C. M.; Schultz, D. E.; Simon, A. J.; Gwinn, E. G. Chiral Electronic Transitions in Fluorescent Silver Clusters Stabilized by DNA. *ACS Nano* **2014**, *8*, 6883−6892.
(28) Copp, S. M.; Schultz, D.; Swasey, S.; Pavlovich, J.; Debord, M.; Chiu, A.; Olsson, K.; Gwinn, E. Magic Numbers in DNA-Stabilized Fluorescent Silver Clusters Lead to Magic Colors. *J. Phys. Chem. Lett.* **2014**, *5*, 959−963.
(29) Xiao, Y.; Shu, F.; Wong, K.-Y.; Liu, Z. Förster Resonance Energy Transfer-Based Biosensing Platform with Ultrasmall Silver Nanoclusters as Energy Acceptors. *Anal. Chem.* **2013**, *85*, 8493−8497.
(30) Kalinin, S.; Peulen, T.; Sindbert, S.; Rothwell, P. J.; Berger, S.; Restle, T.; Goody, R. S.; Gohlke, H.; Seidel, C. A. M. A toolkit and benchmark study for FRET-restrained high-precision structural modeling. *Nat. Methods* **2012**, *9*, 1218−1225.
(31) Förster, T. h. *Ann. Phys.* **1948**, *437*, 55.
(32) Copp, S. M.; Schultz, D.; Swasey, S. M.; Faris, A.; Gwinn, E. G. Cluster Plasmonics: Dielectric and Shape Effects on DNA-Stabilized Silver Clusters. *Nano Lett.* **2016**, *16*, 3594−3599.
(33) Hsu, H.-C.; Ho, M.-C.; Wang, K.-H.; Hsu, Y.-F.; Chang, C.-W. DNA stabilized silver nanoclusters as the fluorescent probe for studying the structural fluctuations and the solvation dynamics of human telomeric DNA. *New J. Chem.* **2015**, *39*, 2140−2145.
(34) Copp, S. M.; Faris, A.; Swasey, S. M.; Gwinn, E. G. Heterogeneous Solvatochromism of Fluorescent DNA-Stabilized Silver Clusters Precludes Use of Simple Onsager-Based Stokes Shift Models. *J. Phys. Chem. Lett.* **2016**, *7*, 698−703.
(35) Thyrhaug, E.; Bogh, S. A.; Carro-Temboury, M. R.; Madsen, C. S.; Vosch, T.; Zigmantas, D. Ultrafast coherence transfer in DNA-templated silver nanoclusters. *Nat. Commun.* **2017**, *8*, No. 15577.

DOI: 10.1021/acsomega.7b00582
ACS Omega 2017, 2, 4657−4664

(36) Values from https://www.thermofisher.com/dk/en/home/references/molecular-probes-the-handbook/technical-notes-and-product-highlights/the-alexa-fluor-dye-series.html.
(37) Würth, C.; Grabolle, M.; Pauli, J.; Spieles, M.; Resch-Genger, U. Relative and absolute determination of fluorescence quantum yields of transparent samples. *Nat. Protoc.* **2013**, *8*, 1535−1550.
(38) Magde, D.; Wong, R.; Seybold, P. G. Fluorescence Quantum Yields and Their Relation to Lifetimes of Rhodamine 6G and Fluorescein in Nine Solvents: Improved Absolute Standards for Quantum Yields. *Photochem. Photobiol.* **2002**, *75*, 327−334.
(39) Brouwer, A. M. Standards for photoluminescence quantum yield measurements in solution (IUPAC Technical Report). *Pure Appl. Chem.* **2011**, *83*, 2213−2228.
(40) Values from https://www.thermofisher.com/dk/en/home/references/molecular-probes-the-handbook/tables/fluorescence-quantum-yields-and-lifetimes-for-alexa-fluor-dyes.html.
(41) Markešević, N.; Oemrawsingh, S. S. R.; Schultz, D.; Gwinn, E. G.; Bouwmeester, D. Polarization Resolved Measurements of Individual DNA-Stabilized Silver Clusters. *Adv. Opt. Mater.* **2014**, *2*, 765−770.
(42) Sens, R.; Drexhage, K. H. Fluorescence quantum yield of oxazine and carbazine laser dyes. *J. Lumin.* **1981**, *24*−*25*, 709−712.
(43) Vosch, T.; Antoku, Y.; Hsiang, J. C.; Richards, C. I.; Gonzalez, J. I.; Dickson, R. M. Strongly emissive individual DNA-encapsulated Ag nanoclusters as single-molecule fluorophores. *Proc. Natl. Acad. Sci. U.S.A.* **2007**, *104*, 12616−12621.
(44) Volkov, I. L.; Serdobintsev, P. Y.; Kononov, A. I. DNA-Stabilized Silver Nanoclusters with High Yield of Dark State. *J. Phys. Chem. C* **2013**, *117*, 24079−24083.
(45) Volkov, I.; Sych, T.; Serdobintsev, P.; Reveguk, Z.; Kononov, A. Fluorescence saturation spectroscopy in probing electronically excited states of silver nanoclusters. *J. Lumin.* **2016**, *172*, 175−179.
(46) Lakowicz, J. R. *Principles of Fluorescence Spectroscopy*, 3rd ed.; Springer, 2006.
(47) Ghiggino, K. P.; Lee, A. G.; Meech, S. R.; O'Connor, D. V.; Phillips, D. Time-resolved emission spectroscopy of the dansyl fluorescence probe. *Biochemistry* **1981**, *20*, 5381−5389.
(48) Toptygin, D.; Brand, L. Spectrally- and time-resolved fluorescence emission of indole during solvent relaxation: a quantitative model. *Chem. Phys. Lett.* **2000**, *322*, 496−502.
(49) Carro Temboury, M. R.; Paolucci, V.; Hooley, E. N.; Latterini, L.; Vosch, T. Probing DNA-stabilized fluorescent silver nanocluster spectral heterogeneity by time-correlated single photon counting. *Analyst* **2016**, *141*, 123−130.
(50) Andreatta, D.; Pérez Lustres, J. L.; Kovalenko, S. A.; Ernsting, N. P.; Murphy, C. J.; Coleman, R. S.; Berg, M. A. Power-Law Solvation Dynamics in DNA over Six Decades in Time. *J. Am. Chem. Soc.* **2005**, *127*, 7270−7271.
(51) Andreatta, D.; Sen, S.; Pérez Lustres, J. L.; Kovalenko, S. A.; Ernsting, N. P.; Murphy, C. J.; Coleman, R. S.; Berg, M. A. Ultrafast Dynamics in DNA: "Fraying" at the End of the Helix. *J. Am. Chem. Soc.* **2006**, *128*, 6885−6892.
(52) Fron, E.; Puhl, L.; Oesterling, I.; Li, C.; Müllen, K.; De Schryver, F. C.; Hofkens, J.; Vosch, T. Energy Transfer Pathways in a Rylene-Based Triad. *ChemPhysChem* **2011**, *12*, 595−608.
(53) Wahl, M. Time-Correlated Single Photon Counting. https://www.picoquant.com/images/uploads/page/files/7253/technote_tcspc.pdf.
(54) Ranjit, S.; Levitus, M. Probing the Interaction Between Fluorophores and DNA Nucleotides by Fluorescence Correlation Spectroscopy and Fluorescence Quenching. *Photochem. Photobiol.* **2012**, *88*, 782−791.

DOI: 10.1021/acsomega.7b00582
ACS Omega 2017, 2, 4657−4664